Magnetic-Mediated Carrier, Phonon and Spin Dynamics in the Ferromagnetic Semiconductor (In,Fe)Sb

K. Hu[1], X. H. Zhu[1], H. L. Wang[2], D. H. Wei[2*], and J. Qi[1*]

[1]*State Key Laboratory of Electronic Thin Films and Integrated Devices, University of Electronic Science and Technology of China, Chengdu 611731, China*
[2]*State Key Laboratory of Semiconductor Physics and Chip Technologies, Institute of Semiconductors, Chinese Academy of Sciences, Beijing 100083, China*

(Received 3 March 2025; accepted manuscript online 1 April 2025)

We investigate the carrier, phonon, and spin dynamics in the ferromagnetic semiconductor (In,Fe)Sb using ultrafast optical pump-probe spectroscopy. We discover two anomalies near T^*(∼40 K) and $T^\dagger$(∼200 K) in the photoexcited carrier dynamics, which can be attributed to the electron-spin and spin-lattice scattering processes influenced by the magnetic phase transition and modifications in magnetic anisotropy. The magnetization change can be revealed by the dynamics of coherent acoustic phonon. We also observe abrupt changes in the photoinduced spin dynamics near T^* and $T^\dagger$, which not only illustrate the spin-related scatterings closely related to the long-range magnetic order, but also reveal the D'yakonov–Perel and Elliott–Yafet mechanisms dominating at temperatures below and above $T^\dagger$, respectively. Our findings provide important insights into the nonequilibrium properties of the photoexcited (In,Fe)Sb.

DOI: 10.1088/0256-307X/42/5/057502 CSTR: 32039.14.0256-307X.42.5.057502

Magnetic semiconductors have attracted significant interest due to their potential applications in semiconductor spintronics.[1–3] It is noteworthy that these materials exhibit characteristics of both semiconductors and ferromagnets.[4] In the past two decades, many important results have been obtained for Ⅲ-Ⅳ semiconductors heavily doped with Mn.[2,5–8] However, Mn-doped Ⅲ-Ⅴ semiconductors are always p-type and exhibit a Curie temperature much lower than room temperature. To overcome these limitations, Fe-doped narrow-gap semiconductors such as n-type (In,Fe)Sb and p-type (Ga,Fe)Sb[9–11] have attracted great interest.

In particular, many studies have confirmed that the Curie temperature of Fe- or Ni-doped InSb can be close to or even above room temperature at sufficiently high Fe concentrations.[9–12] (In,Fe)Sb also exhibits a large anomalous Hall effect,[12,13] which may be applied to magnetic-field sensors with ultrahigh Hall sensitivity. Furthermore, numerous studies have also been conducted on the physical properties of (In,Fe)Sb to unravel its ferromagnetism.[14–16] However, so far the nonequilibrium carrier, phonon and spin dynamics of (In,Fe)Sb have never been explored. Clarifying the dynamics of its photoexcited state is not only important for the fundamental physics of magnetic semiconductors, but also for future applications in spintronics and opto-electronics using this type of material.

In this work, for the first time we report the systematic study of ultrafast carrier, phonon and spin dynamics in (In,Fe)Sb using time-resolved optical reflectivity and Kerr rotation measurements. Our results reveal the electron-phonon (e-ph) scattering, electron-spin (e-s) scattering, and spin-lattice (s-l) coupling processes dominating the initial relaxation of photoexcited (In,Fe)Sb system. Changes in the magnetic properties of this material near two critical temperatures, T^*(∼40 K) and $T^\dagger$(∼200 K), are clearly disclosed via the spin-related scatterings. In addition, change in the magnetization property near T^* can also be revealed via analyzing the dynamics of coherent acoustic phonons.

The (In,Fe)Sb film was grown on a semi-insulating GaAs(001) substrate with several additional buffer layers by the low-temperature molecular beam epitaxy technique[12] [see the sample details in the Supplementary Materials (SM)]. Measurements of magnetic properties reveal its ferromagnetic properties persisting up to ∼320 K (see SM). The optical transient reflectivity $\Delta R(t)/R$ from 5 K to room temperature was measured using a Ti:sapphire femtosecond (fs) laser with a pulse width of ∼35 fs and a repetition rate of 80 MHz at a center wavelength of 800 nm (∼1.55 eV). During measurements, the pump beam, with a typical fluence of ∼0.8 μJ/cm^2, was directed along the normal incidence and kept p-polarized. The probe beam was incident at a small angle to the sample normal and kept s-polarized. The power ratio between pump and probe was 10:1. Additional information about the experimental setup can be found in Refs. [17,18].

Figure 1(a) shows the typical transient reflectivity $\Delta R(t)/R$ data at several temperatures. After photoexcitation, an instantaneous rise can be clearly observed at all investigated temperatures, followed by the subsequent relaxation processes. Besides, as shown in Figs. 1(a) and

*Corresponding author. Email: dhwei@semi.ac.cn; jbqi@uestc.edu.cn
© 2025 Chinese Physical Society and IOP Publishing Ltd. All rights, including for text and data mining, AI training, and similar technologies, are reserved.

1(c), the obvious damped oscillations, with frequencies in both terahertz (THz) and gigahertz (GHz) regimes, are superimposed on the non-oscillating background.

We first focus on the non-oscillatory signals, a typical fitting of $\Delta R(t)/R$ using two decay components. In order to extract the relaxation time, the $\Delta R(t)/R$ signals before 10 ps are fitted using the following formula:[19,20]

$$\Delta R(t)/R = \left(\sum_{j=1,2} A_j e^{-t/\tau_j} + C \right) \otimes G(t), \qquad (1)$$

where A_j and τ_j represent the amplitude and relaxation time of the jth decay component, respectively. C is a constant, and $G(t)$ is a Gaussian function representing the pump-probe cross-correlation. As shown in Fig. 1(b), the fitted curves are in excellent agreement with the experimental data. τ_1 and τ_2, characterizing the fast and slower relaxation processes, are strongly temperature dependent. In order to gain insight into origin of the two decay processes, we have done a careful examination of the temperature-dependent τ_1 and τ_2 [see Figs. 1(d) and 1(e)].

In general, after electron-electron thermalization, hot carriers begin to transfer their excess energy to the lattice system with a sub-picosecond (sub-ps) timescale via e-ph scattering in metals and semiconductors.[20–23] Here, τ_1 is less than 1 ps, and hence its associated process should be closely related to the e-ph scattering, which can be phenomenologically described by the two-temperature model (TTM).[23,24] Figure 1(d) illustrates the fitted results for τ_1 using TTM, which is not valid for $T \lesssim \theta_D/5$ ($\theta_D \approx 500$ K)[25–27] (see fitting details in SM). It can be seen that experimental data between ∼100 and 200 K agree well with the fitting. However, apparent anomalies emerge around T^*(∼40 K) in both τ_1 and τ_2. Discrepancy also exists between the fitted curves and the experimental data at $T > 200$ K.

Since (In,Fe)Sb is a ferromagnetic semiconductor, the spin degree of freedom cannot be neglected. In fact, the e-s scattering has a similar timescale as that of the e-ph thermalization in different types of magnetic materials.[28–30] Therefore, τ_1 can also contain information from both e-ph and e-s scatterings. The spin degree of freedom can still play a vital role in the timescales from ps to ns,[29–31] which is believed to arise from the s-l coupling. Therefore, we need to consider this mechanism to clarify the T-dependent τ_2.

Actually, in the data of magnetization versus temperature (M–T), peculiar behavior is also observed around 40 K (see SM). Specifically, M experiences a sharp increase below ∼40 K in the in-plane M–T curve, suggesting the emergence of a secondary ferromagnetic phase or the existence of magnetic phase separation below T^*, which is very similar to the observation in other magnetic materials.[32] If this phase separation appears below T^*, an additional e-s scattering channel will open. It can further compromise the e-ph scattering, and lead to saturation of τ_1. Simultaneously, due to the s-l scattering time proportional to $[1/C_l + 1/C_s]^{-1}$,[33] where C_l and C_s are the lattice and spin heat capacities, respectively, τ_2 will also maximize at T^* since $C_s(T)$ will peak around the transition temperature. These two behaviors are fully consistent with our observation, and confirm the suggested scenario emerging at low temperatures in (In,Fe)Sb.

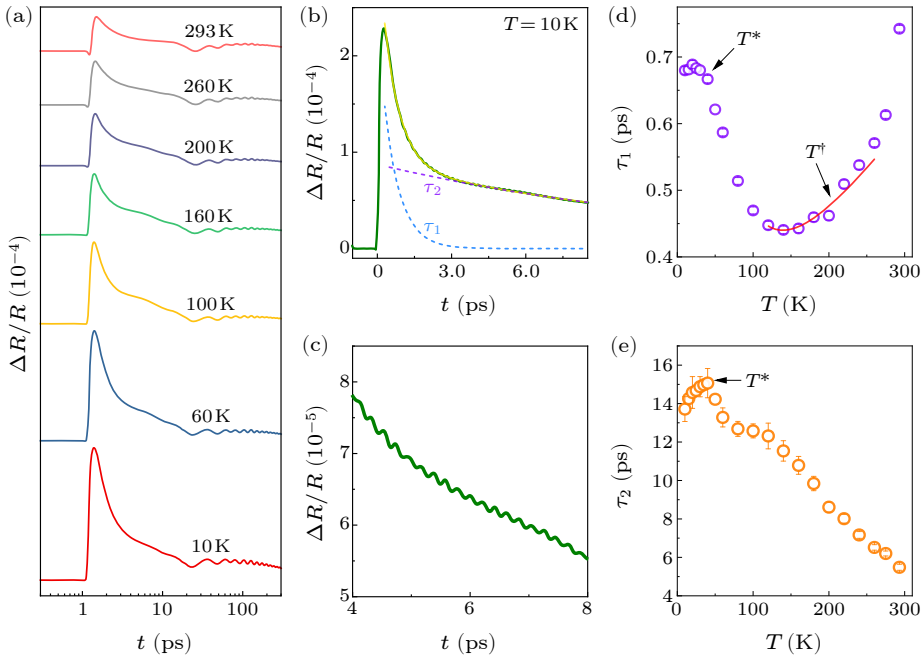

Fig. 1. (a) Typical $\Delta R(t)/R$ signals of (In,Fe)Sb at various temperatures. (b) A typical fitting of $\Delta R(t)/R$ using two exponential decays shown by the yellow line. The short dashed lines represent the contributions of two decay processes obtained from the fitting. (c) The high-frequency oscillations in $\Delta R(t)/R$ signals. (d) τ_1 as a function of temperature. The bright red solid curve denotes the TTM fit. (e) τ_2 as a function of temperature. The black arrows indicate the anomalies in τ_1 and τ_2 around T^* and $T^\dagger$.

Furthermore, the in-plane and out-of-plane M-T curves demonstrate that the magnetic anisotropy experiences a severe change around 200 K, and indicate the emergence of possible spin-reorientation near this temperature. Since the e-s scattering is very sensitive to the change of magnetic and electronic structure,[34] it is reasonable that τ_1 deviates from TTM above ∼200 K, as seen in Fig. 1(d). This transition will be further manifested in the spin dynamics discussed later.

We now focus on the oscillatory part of $\Delta R(t)/R$. Figures 2(a) and 2(b) plot the high-frequency oscillations extracted from the decay process after subtracting the nonoscillatory background. Three distinct THz modes are observed, including $\omega_1/2\pi$ ∼4.7 THz, $\omega_2/2\pi$ ∼5.8 THz, and $\omega_3/2\pi$ ∼7 THz. These oscillations with THz frequency usually result from coherent optical phonons triggered by displacive excitation or Raman scattering.[35,36] Except for these three frequencies, the Raman spectroscopy of (In,Fe)Sb also reveals phonons at additional frequencies (see SM), which are generally modes associated with the asymmetric E_g phonons that could decay extremely fast in the time domain.[37] Here, ω_1, ω_2, and ω_3 can be identified as the coherent A_g^1 phonon modes.

In order to explore properties of the coherent phonon modes, we use the following equation to fit the time-domain oscillatory signals:

$$(\Delta R(t)/R)_{\rm osc} = \sum_{j=1,2,3} B_j e^{-t*\Gamma_j} \sin(\omega_j t + \phi_j), \quad (2)$$

where B_j, Γ_j, $\omega_j/2\pi$, and ϕ_j are the amplitude, damping rate, frequency, and phase of the three modes, respectively. The temperature-dependent evolutions of ω_j and Γ_j are shown in Figs. 2(c) and 2(d). $\omega_j(T)$ and $\Gamma_j(T)$, in general, can be described by the anharmonic phonon decay process given by[20,22,38,39]

$$\omega^{\text{ph-ph}}(T) = \omega_0 + a\left[1 + 2n_B\left(\frac{\omega_0}{2}, T\right)\right], \quad (3)$$

$$\Gamma^{\text{ph-ph}}(T) = \Gamma_0 + b\left[1 + 2n_B\left(\frac{\omega_0}{2}, T\right)\right], \quad (4)$$

where $\omega_0/2\pi$ and Γ_0 are the intrinsic frequency and damping rate, respectively. a and b are the fitting parameters. $n_B(\omega, T)$ is the Bose–Einstein distribution function. As shown in Fig. 2, our experimental data can be well explained by the anharmonic effect of optical phonons, and also indicate that the spin degree of freedom is not coupled with the THz optical phonon.

Next, we analyze the low-frequency oscillatory component in the GHz range, as shown in Fig. 1(a) and Fig. 3(a). In heterostructure semiconductors, this type of oscillation, clearly seen in the timescale of ∼10 ps, conventionally arises from the propagating coherent longitudinal acoustic wave generated on the sample surface via excitation of the fs laser pulse, and its frequency can be described by[40,41] $f = 2nV_s/\lambda$. Here, f, n, λ, and V_s are the frequency of oscillation, refractive index, wavelength of the probe light, and sound velocity, respectively.

The frequency change can be clearly noticed in the temperature-dependent oscillatory components [Fig. 3(a)]. Its detailed dependence on T is illustrated by the $1/f$ vs. T curve in Fig. 3(b).[42] Clearly, $1/f$, in general, decreases with decreasing T, and almost saturates below T^* or above $T^\dagger$. Based on $f = 2nV_s/\lambda$, such T-dependence could be attributed to the effective change of nV_s. Therefore, in a large temperature range, change of $1/f(T)$ is a joint effect of n and V_s. Based on the previous experiments in Ⅲ-Ⅴ ferromagnetic semiconductor GaMnAs,[41] V_s becomes smaller as T decreases. In some temperature regimes, e.g., below ∼ T^*, $1/f$ can show saturation behavior if the decrease of V_s is compensated by the increase of n. It is obvious that the changes of magnetic properties play the key role, and its clarification requires detailed theoretical investigation in the future.

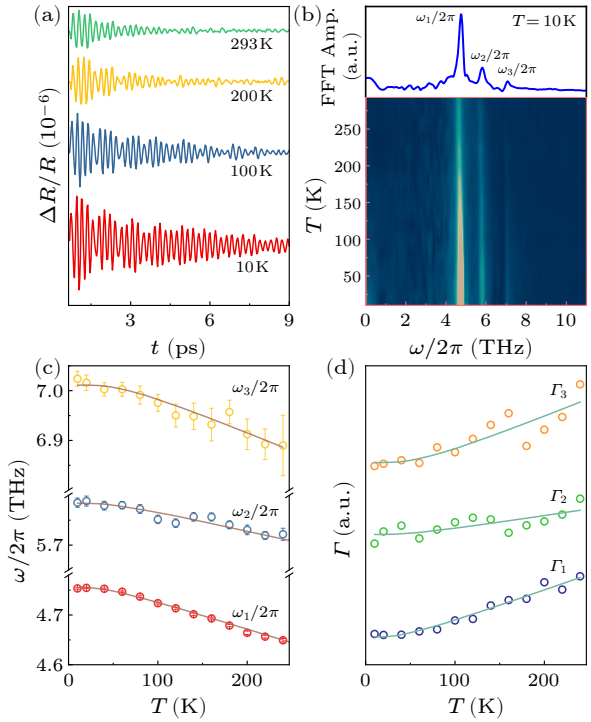

Fig. 2. (a) Extracted high-frequency oscillations at four typical temperatures: 10, 100, 200, and 293 K. (b) The Fourier transform spectra for the extracted oscillations from room temperature down to 10 K. (c) and (d) show the frequency $\omega_j/2\pi$ (j = 1, 2, 3) and damping rate Γ_j (j = 1, 2, 3) of different phonon modes as functions of temperature. The solid lines represent the fitting results using the anharmonic phonon model.

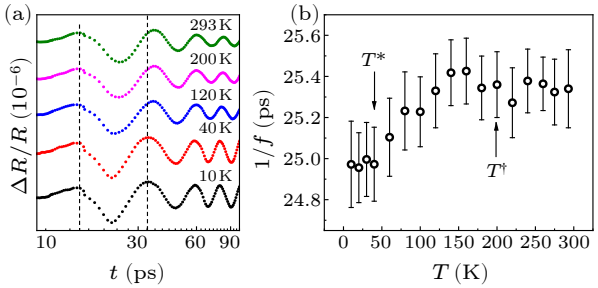

Fig. 3. (a) Extracted low-frequency oscillation components at five typical temperatures: 10, 40, 120, 200, and 293 K. (b) The derived period, $1/f$, as a function of temperature. The black arrows represent the two critical temperatures as T^* and $T^\dagger$.

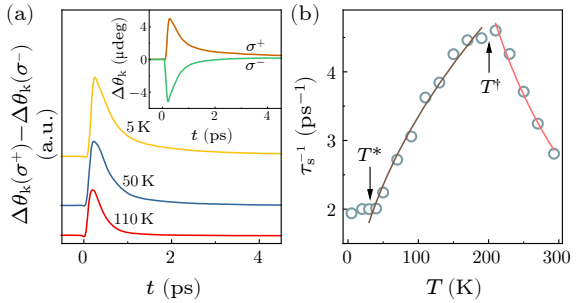

Fig. 4. (a) The Kerr rotation signals for $\Delta\theta_k(\sigma^+) - \Delta\theta_k(\sigma^-)$ at several typical temperatures. The inset shows the time-resolved Kerr rotation signals, $\Delta\theta_k$, for left (σ^+) and right (σ^-) circularly polarized lights at 5 K. (b) The spin decay rate τ_s^{-1} as a function of temperature. The solid lines represent the fitting with different mechanisms using Eq. (5). The black arrows indicate the anomalies around T^* and $T^\dagger$.

At last, we discuss the photo-induced spin dynamics, which is accomplished by measuring the time-resolved Kerr rotation via excitation of the circularly polarized light.[17] The inset of Fig. 4(a) shows typical measurements of Kerr rotation angle, $\Delta\theta_k(t)$, at 5 K. Due to $\Delta\theta_k(t) \propto \langle \boldsymbol{s} \rangle$, it can be seen that the circularly polarized light is capable of generating a net spin polarization decaying as a function of time in the sample. Moreover, the polarization direction reflected by Kerr rotation angle changes sign with the helicity of pump light. Microscopically, the generation of a net spin density in opaque materials by circularly polarized light involves direct optical transitions between different energy levels and the accompanying angular momentum transfer (spin selection rules).[17,43] Therefore, to understand the spin dynamics, we have carried out detailed measurements on the temperature-dependent Kerr rotation, $\Delta\theta_k(\sigma^+) - \Delta\theta_k(\sigma^-)$. Typical data are shown in Fig. 4(a). The spin relaxation time, τ_s, is obtained by fitting the experimental data using a single exponential decay, as shown in Fig. 4(b). Evident anomalies can be found near T^* and $T^\dagger$.

Since (In,Fe)Sb is a Ⅲ-Ⅴ ferromagnetic semiconductor, it should contain two different spin relaxation mechanisms, D'yakonov–Perel (DP) mechanism[44] and Elliott–Yafet (EY) mechanism.[45] The former explains spin dephasing in solids without a center of symmetry. Spin dephasing occurs because electrons feel an effective magnetic field, resulting from the lack of inversion symmetry and the spin-orbit interaction. This magnetic field changes in random directions every time the electron scatters to a different momentum state. In the latter, electron spins relax because the electron wave functions normally associated with a given spin have an admixture of the opposite-spin states, due to spin-orbit coupling induced by the ions.[34] Thus, the temperature-dependent spin decay rate including both mechanisms can be written as[46]

$$\frac{1}{\tau_s} = \frac{1}{\tau_s^{DP}} + \frac{1}{\tau_s^{EY}} = A\,T^{\alpha} + B\,T^{-1} + C, \qquad (5)$$

where τ_s is the spin relaxation time, α, A, and B are fitting parameters. Note that $(\tau_s^{DP})^{-1} \propto \tau_p$,[34] where τ_p is the momentum scattering time and $\tau_p \propto T^{\alpha}$. Here, α is 1/2 or 3/2 if the scattering is dominated by optical and acoustic phonons, respectively.

In order to get a good fit for $\tau_s(T)$, we employ a segmental fitting below and above $T^\dagger$, i.e., $A = 0$ for $T \gtrsim 200$ K and $B = 0$ for $T \lesssim 200$ K. The fitted curves are shown in Fig. 4(b). The former indicates that the EY mechanism is prevailing, while the latter suggests that the DP mechanism is playing a more important role. Specifically, we obtain α to be ∼1/2, which indicates the optical phonon scattering dominates the spin relaxation in the DP mechanism. Nonetheless, our results reveal that the spin reorientation or change of magnetic anisotropy across a critical temperature could be microscopically connected to the detailed spin scattering mechanism in the ferromagnetic semiconductor. In addition, fluctuation of localized magnetic moments will strongly affect the spin scattering of electrons.[47] Below the phase transition temperature, the fluctuation is frozen at some degree, and hence is capable of saturating the spin relaxation time τ_s. This might explain the anomaly near T^*.

In summary, our study employs ultrafast optical pump-probe spectroscopy to investigate carrier, phonon, and spin dynamics in the ferromagnetic semiconductor (In,Fe)Sb. We identify two anomalous features in the relaxation process of photoexcited carriers near critical temperatures T^*(∼40 K) and $T^\dagger$(∼200 K). These anomalies can be ascribed to changes in e-s scattering and s-l coupling processes, driven by the onset of magnetic phase transitions and shifts in magnetic anisotropy. Analysis of coherent acoustic phonon dynamics also reveals the magnetization change as a function of temperature. Additionally, abrupt changes in spin lifetime observed at T^* and $T^\dagger$ not only reveal the influence of evolving long-range magnetic order but also show the detailed spin scattering mechanisms varying in different temperature regimes. These findings offer critical insights into the nonequilibrium properties of photoexcited magnetic semiconductors and uncover their potential applications in next-generation spintronic and optoelectronic devices.

Acknowledgements. We thank Dr. Wenshuai Gao for his help in measuring the magnetic properties. This work was supported by the National Key R&D Program of China (Grant No. 2024YFA1408502), the National Natural Science Foundation of China (Grant Nos. 92365102, 62027807, 12474107, and 12174383), the Chinese Academy of Sciences project for Yong Scientists in Basic Research (Grant No. YSBR-030), and the Guangdong Basic and Applied Basic Research Foundation (Grant No. 2024A1515011600).

References

[1] Haury A, Wasiela A, Arnoult A, Cibert J, Tatarenko S, Dietl T, and Merle d'Aubigné Y 1997 *Phys. Rev. Lett.* **79** 511

[2] Ertler C, Matos-Abiague A, Gmitra M, Turek M, and Fabian J 2008 *J. Phys: Conf. Ser.* **129** 012021

[3] Tanaka M 2020 *Jpn. J. Appl. Phys.* **60** 010101

[4] Holub M and Bhattacharya P 2007 *J. Phys. D: Appl. Phys.* **40** R179
[5] Ohno H, Chiba D, Matsukura F, Omiya T, Abe E, Dietl T, Ohno Y, and Ohtani K 2000 *Nature* **408** 944
[6] Sato K, Bergqvist L, Kudrnovský J, Dederichs P H, Eriksson O, Turek I, Sanyal B, Bouzerar G, Katayama-Yoshida H, Dinh V A, Fukushima T, Kizaki H, and Zeller R 2010 *Rev. Mod. Phys.* **82** 1633
[7] Matsukura F, Ohno H, Shen A, and Sugawara Y 1998 *Phys. Rev. B* **57** R2037
[8] Dinh V A, Sato K, and Katayama-Yoshida H 2003 *Jpn. J. Appl. Phys.* **42** L888
[9] Sriharsha K, Anh L D, Tu N T, Goel S, and Tanaka M 2019 *APL Mater.* **7** 021105
[10] Tu N T, Hai P N, Anh L D, and Tanaka M 2016 *Appl. Phys. Lett.* **108** 192401
[11] Goel S, Anh L D, Tu N T, Ohya S, and Tanaka M 2019 *Phys. Rev. Mater.* **3** 084417
[12] Deng Z, Wang H, Wei Q, Liu L, Sun H, Pan D, Wei D, and Zhao J 2024 *J. Semicond.* **45** 012101
[13] Nishijima K, Tu N T, Tanaka M, and Hai P N 2019 *J. Cryst. Growth* **511** 127
[14] Tu N T, Hai P N, Anh L D, and Tanaka M 2018 *Appl. Phys. Express* **11** 063005
[15] Shinya H, Fukushima T, Masago A, Sato K, and Katayama-Yoshida H 2018 *J. Appl. Phys.* **124** 103902
[16] Tu N T, Hai P N, Anh L D, and Tanaka M 2018 *Appl. Phys. Lett.* **112** 122409
[17] Wang M C, Qiao S, Jiang Z, Luo S N, and Qi J 2016 *Phys. Rev. Lett.* **116** 036601
[18] Liu Y P, Zhang Y J, Dong J J, Lee H, Wei Z X, Zhang W L, Chen C Y, Yuan H Q, Yang Y F, and Qi J 2020 *Phys. Rev. Lett.* **124** 057404
[19] Hilton D J and Tang C L 2002 *Phys. Rev. Lett.* **89** 146601
[20] Cheng L, Fei F C, Hu H, Dai Y M, Song F Q, and Qi J 2022 *Phys. Rev. B* **106** 104308
[21] Wu Q, Sun F, Zhang Q, Zhao L X, Chen G F, and Zhao J 2020 *Phys. Rev. Mater.* **4** 064201
[22] Qi J, Chen X, Yu W, Cadden-Zimansky P, Smirnov D, Tolk N H, Miotkowski I, Cao H, Chen Y P, Wu Y, Qiao S, and Jiang Z 2010 *Appl. Phys. Lett.* **97** 182102
[23] Allen P B 1987 *Phys. Rev. Lett.* **59** 1460
[24] Groeneveld R H M, Sprik R, and Lagendijk A 1990 *Phys. Rev. Lett.* **64** 784
[25] Hase M, Ishioka K, Demsar J, Ushida K, and Kitajima M 2005 *Phys. Rev. B* **71** 184301
[26] Demsar J, Averitt R D, Ahn K H, Graf M J, Trugman S A, Kabanov V V, Sarrao J L, and Taylor A J 2003 *Phys. Rev. Lett.* **91** 027401
[27] Groeneveld R H M, Sprik R, and Lagendijk A 1995 *Phys. Rev. B* **51** 11433
[28] Beaurepaire E, Merle J C, Daunois A, and Bigot J Y 1996 *Phys. Rev. Lett.* **76** 4250
[29] Kirilyuk A, Kimel A V, and Rasing T 2010 *Rev. Mod. Phys.* **82** 2731
[30] Jungwirth T, Wunderlich J, Novák V, Olejník K, Gallagher B L, Campion R P, Edmonds K W, Rushforth A W, Ferguson A J, and Němec P 2014 *Rev. Mod. Phys.* **86** 855
[31] Wu M W, Jiang J H, and Weng M Q 2010 *Phys. Rep.* **493** 61
[32] Kang J, Yang Y, Qian X, Xu K, Cui X, Fang Y, Chandragiri V, Kang B, Chen B, Stroppa A, Cao S, Zhang J, and Ren W 2017 *IUCrJ* **4** 598
[33] Cheng L, Xiang T, and Qi J 2024 *Phys. Rev. Res.* **6** 023073
[34] Žutić I, Fabian J, and Das Sarma S 2004 *Rev. Mod. Phys.* **76** 323
[35] Merlin R 1997 *Solid State Commun.* **102** 207
[36] Zeiger H J, Vidal J, Cheng T K, Ippen E P, Dresselhaus G, and Dresselhaus M S 1992 *Phys. Rev. B* **45** 768
[37] O'Mahony S M, Murphy-Armando F, Murray É D, Querales-Flores J D, Savić I, and Fahy S 2019 *Phys. Rev. Lett.* **123** 087401
[38] Balkanski M, Wallis R F, and Haro E 1983 *Phys. Rev. B* **28** 1928
[39] Menéndez J and Cardona M 1984 *Phys. Rev. B* **29** 2051
[40] Thomsen C, Grahn H T, Maris H J, and Tauc J 1986 *Phys. Rev. B* **34** 4129
[41] Qi J, Yan J A, Park H, Steigerwald A, Xu Y, Gilbert S N, Liu X, Furdyna J K, Pantelides S T, and Tolk N 2010 *Phys. Rev. B* **81** 115208
[42] Considering a typical value of sound velocity (∼4000 m/s) for Ⅲ–V semiconductors and the acoustic wave's back-reflection from the air-sample interface, we only use two periods of the oscillation data to extract $1/f$, which is good energh to reveal the properties of (In, Fe)Sb. The oscillatory behavior thereafter will mostly represent the acoustic wave traveling further into (In, Ga)Sb, (Al, Ga)Sb and so on.
[43] Planel R and Guillaume C B A L 1984 *Modern Problems in Condensed Matter Sciences* (Elsevier) **8** p. 353
[44] Dyakonov M I and Perel V I 1971 *Phys. Lett. A* **35** 459
[45] Elliott R J 1954 *Phys. Rev.* **96** 266
[46] Han W and Kawakami R K 2011 *Phys. Rev. Lett.* **107** 047207
[47] Niimi Y, Wei D H, and Otani Y 2017 *J. Phys. Soc. Jpn.* **86** 011004